

1 **Influence of bank slope on sinuosity-driven hyporheic exchange flow and**  
2 **residence time distribution during a dynamic flood event**

3

4 **Supporting Information**

5

6 Yiming Li<sup>1,2</sup>, Uwe Schneidewind<sup>2</sup>, Zhang Wen<sup>1\*</sup>, Stefan Krause<sup>2</sup>, Hui Liu<sup>1</sup>

7

8 <sup>1</sup>Hubei Key Laboratory of Yangtze River Catchment Environmental Aquatic Science,  
9 School of Environmental Studies, China University of Geosciences, People's Republic  
10 of China

11 <sup>2</sup>School of Geography, Earth and Environmental Sciences, University of Birmingham,  
12 UK

13

14 **\*Correspondence:** Zhang Wen ([wenz@cug.edu.cn](mailto:wenz@cug.edu.cn))

15 This supporting information contains additional information on how the model used in  
 16 our simulations was set up in COMSOL. Our modeling approach builds on the work of  
 17 Gomez-Velez et al. (2017), which serves as a baseline case. Due to their large file size  
 18 the COMSOL model files and the raw data to the figures in the manuscript are available  
 19 upon request and we are delighted to share them directly. For this please contact Yiming  
 20 Li (liy@cug.edu.cn) or Zhang Wen (wenz@cug.edu.cn).

## 21 **S1 Water flow model**

22 The water flow model is based on that of Gomez-Velez et al. (2017), comprising  
 23 an alluvial valley with a sinusoidal meandering river that overlies non-permeable river  
 24 deposits, as shown in Fig. S1. To simplify the model, aquifer properties are assumed to  
 25 be spatially homogeneous and isotropic. This means they can be modeled by the  
 26 commonly used vertical-integrated approach which can reduce a 3-D groundwater flow  
 27 to a two-dimensional (2-D) problem, as shown in Fig. S2a. The model is bounded by  
 28 hillslopes and a two-period fully penetrating sinusoidal river. By neglecting the  
 29 compression of groundwater, the unsteady, 2-D transient groundwater flow through the  
 30 deformable aquifer is described by the Boussinesq's equation:

$$31 \quad S_y \frac{\partial h}{\partial t} = \nabla [K(h - z_b) \nabla h] \quad (\text{S1a})$$

$$32 \quad h(\mathbf{x}, t = 0) = h_0(\mathbf{x}) \quad (\text{S1b})$$

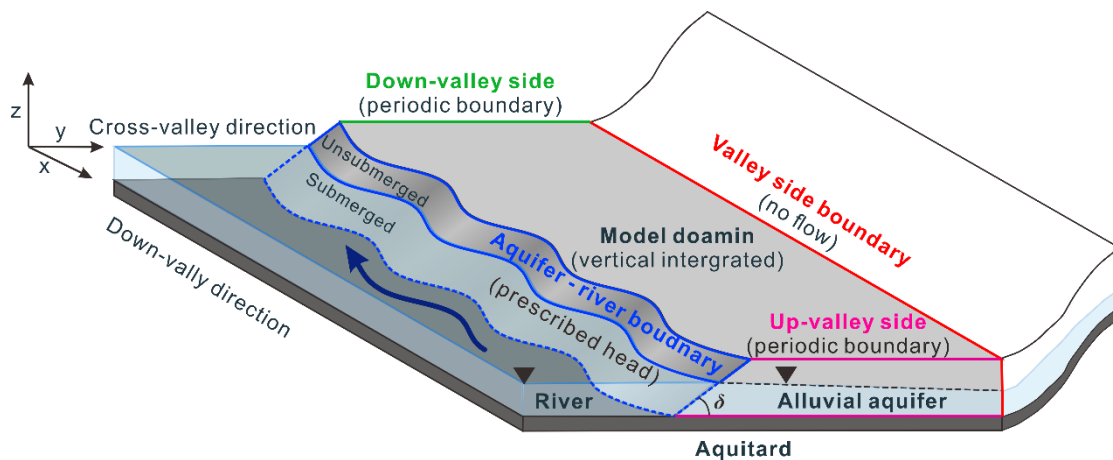
$$33 \quad \mathbf{n} \cdot \nabla [K(h - z_b) \nabla h] = 0 \quad \text{for } \Omega_v \quad (\text{S1c})$$

$$34 \quad h(x_u, y, t) = h(x_d, y, t) + 2 \lambda J_x \quad \text{for } \Omega_u \text{ and } \Omega_d \quad (\text{S1d})$$

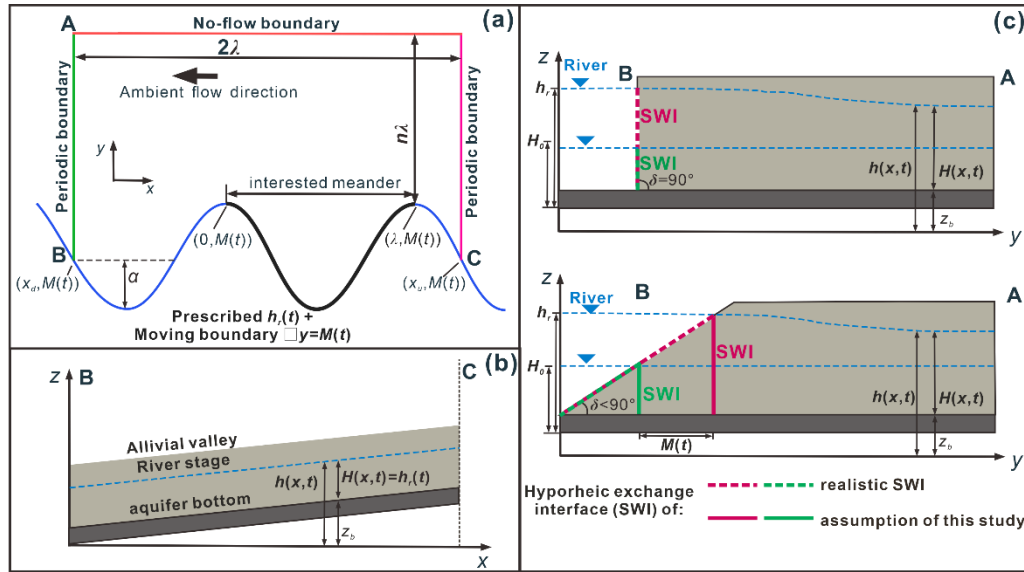
$$35 \quad h(\mathbf{x}, t) = \left(\frac{J_x}{\sigma}\right)s(x) + H_s(t) + 2 \lambda J_x \quad \text{for } \Omega_{in} \cup \Omega_{out} \quad (\text{S1e})$$

36 where  $\mathbf{x} = (x, y)$  [L] is the spatial coordinate with  $x$  positive in the upstream direction,  $t$   
 37 [T] is simulation time,  $S_y$  [-] is specific yield,  $K$  [ $\text{LT}^{-1}$ ] is the hydraulic conductivity,  $\nabla$   
 38 is the Laplace operator,  $h(\mathbf{x}, t)$  and  $h_0(\mathbf{x})$  [L] represent the hydraulic head at  $t$  and  $t = 0$ ,  
 39 while  $z_b(\mathbf{x})$  [L] is the elevation of the underlying impermeable layer with respect to the  
 40 reference datum  $z = 0$  (see Fig. S2b and S2c), respectively.  $H(\mathbf{x}, t) = h(\mathbf{x}, t) - z_b(\mathbf{x})$  [L]

41 is the thickness of the saturated aquifer,  $\mathbf{n}$  is the outward normal vector along the model  
 42 boundary,  $\Omega_v$ ,  $\Omega_u$  and  $\Omega_d$  are the valley, upstream and downstream boundaries,  
 43 respectively, while  $\Omega_{in}$  and  $\Omega_{out}$  are the inlet and outlet boundaries along the river. The  
 44 fluxes are calculated by Darcy's law via:  $\mathbf{q} = -K\nabla h$  [ $LT^{-1}$ ]. Here,  $\mathbf{q}$  is the specific  
 45 discharge or Darcy flux,  $\mathbf{q}/\theta$  [ $LT^{-1}$ ] is the pore water velocity with  $\theta$  [-] as effective  
 46 porosity, and  $\mathbf{Q} = \mathbf{q}(h - z_b)$  [ $L^2T^{-1}$ ] is the aquifer-integrated discharge in our 2-D model.  
 47 The valley boundary ( $\Omega_v$ ) is assigned as a no-flow boundary and located at  $y = n\lambda$ , with  
 48 the scaling number  $n = 4.5$ , which has proven to be sufficiently large for this simulation  
 49 based on a series of pre-simulation tests while  $\lambda$  [L] is the wavelength of the river  
 50 sinusoid. The river has been assigned the known transient hydraulic head,  $h_r(x, t) =$   
 51  $(J_x/\sigma)s(x) + H_r(t)$  [m], where  $J_x$  [-] is the base head gradient of ambient flow along the  
 52 valley in positive  $x$  direction,  $H_r(t)$  [L] is the elevation of river stage above the  
 53 impermeable deposit at the downstream end.  
 54



55  
 56 **Figure S1.** Conceptual model of the study area. Colored lines represent the river, up-  
 57 valley, down-valley and valley side boundary conditions set in the model. Modified  
 58 from Schmadel et al. (2016)  
 59



60

61 **Figure S2.** Modified after Gomez-Velez et al. (2017): (a) Schematic representation of  
 62 the boundary conditions for the non-submerged alluvial system. The colors of the  
 63 boundaries correspond to those in Fig. S1. (b) Representation of the stream stage  
 64 variation along the channel thalweg. (c) Cross-section of unconfined aquifer and  
 65 floodplain of vertical ( $\delta = 90^\circ$ ) and sloping riverbank ( $\delta < 90^\circ$ ). Green and red lines  
 66 refer to the sediment-water interface (SWI) during base flow condition and flood event,  
 67 respectively; the dashed lines on riverbank surface and the vertical bold lines in Fig.  
 68 S2c indicate the realistic SWIs and SWIs of this study, respectively.

69

70 The river ( $\Omega_{in} \cup \Omega_{out}$ ) is implemented as a sinusoid, following the  
 71 conceptualizations of Boano et al. (2016), Cardenas (2009a, 2009b), and Gomez-Velez  
 72 et al. (2017). The initial condition is represented as:  $y_0(x) = \alpha \cos(2\pi x/\lambda) - \alpha$ , where  $\alpha$  [L]  
 73 is the amplitude of the river boundary. Left- and right-bottom vertices in initial  
 74 condition are located at  $x_d = -3\lambda/4$  and  $x_u = 5\lambda/4$ , respectively.

75 The impermeable bottom deposit  $z_b = J_x(x - x_d)$  [L] is assumed to be parallel to  
 76 the alluvial valley.  $\Omega_u$  and  $\Omega_d$  are periodic with a known variable hydraulic head drop  
 77  $h(x = x_u, y, t) = h(x = x_d, y, t) + 2\lambda J_x$  [L] to eliminate any boundary effects. Thus, the  
 78 model domain can represent two periodic parts in horizontal direction of the infinite  
 79 aquifer. The river stage fluctuates during the dynamic flood event following (Cooper

80 and Rorabaugh, 1963):

$$81 \quad H_s = \begin{cases} H_0 + H_p \exp \left\{ -\eta(t-t_p) \frac{[1-\cos(\omega t)]}{[1-\cos(\omega t_p)]} \right\} & \text{if } 0 < t < t_p \\ H_0 & \text{if } t_p < t \end{cases} \quad (\text{S2})$$

82 where  $H_0(\mathbf{x})$  [L] is the initial river stage,  $H_p$  [L] is the maximum (peak) river stage  
 83 during the flood event, while  $t_d$  and  $t_p$  [T] are the duration of flood event and the time-  
 84 to-peak river stage, respectively.  $\omega = 2\pi/t_d$  [T<sup>-1</sup>] is the flood event frequency,  $\eta =$   
 85  $\omega \cot(\omega t_p/2)$  [T<sup>-1</sup>] represents the degree of flood event asymmetry. The peak river stage  
 86 and time-to-peak are assumed to be linearly correlated with the base flow stage ( $H_p =$   
 87  $n_0 H_0$ ) and the duration of the event ( $t_p = n_d t_d$ ), respectively. Constants  $n_0$  [-] and  $n_d$  [-]  
 88 represent river stage hydrograph intensity and skewness.

89

## 90 S2 Conservative solute transport model and calculation of HZ area (extent)

91 In this work, we adopt the mathematical model used by Gomez-Velez et al. (2017),  
 92 where the transport of a conservative solute within the vertically integrated system is  
 93 given by:

$$94 \quad \frac{\partial(H\theta C)}{\partial t} = \nabla \cdot (\mathbf{D}\nabla C - \mathbf{Q}C) \quad (\text{S3a})$$

$$95 \quad C(\mathbf{x}, t=0) = C_0(\mathbf{x}) \quad (\text{S3b})$$

$$96 \quad \mathbf{n} \cdot (\mathbf{Q}C - \mathbf{D}\nabla C) = 0 \text{ for } \Omega_v \quad (\text{S3c})$$

$$97 \quad C(x_u, y, t) = C(x_d, y, t) \text{ for } \Omega_u \text{ and } \Omega_d \quad (\text{S3d})$$

$$98 \quad C(\mathbf{x}, t) = C_s(\mathbf{x}, t) \text{ for } \Omega_{in} \quad (\text{S3e})$$

$$99 \quad \mathbf{n} \cdot (\mathbf{Q}C - \mathbf{D}\nabla C) = 0 \text{ for } \Omega_{out} \quad (\text{S3f})$$

100 where  $C(\mathbf{x}, t)$ ,  $C_0(\mathbf{x})$ , and  $C_s(\mathbf{x}, t)$  are the solute concentrations [ML<sup>-3</sup>] in the aquifer,  
 101 initial concentration and concentration in the river, respectively. The dispersion-  
 102 diffusion tensor  $\mathbf{D} = \{D_{ij}\}$  [L<sup>2</sup>T<sup>-1</sup>] is defined according to Bear and Cheng (2010) as:

103 
$$D_{ij} = \alpha_T |\mathbf{Q}| \delta_{ij} + (\alpha_L - \alpha_T) \frac{Q_i Q_j}{|\mathbf{Q}|} + H\theta\epsilon D_L \quad (\text{S4})$$

104 where  $\alpha_T$  and  $\alpha_L$  [L] are the transverse and longitudinal dispersivity, respectively,  $D_L$   
 105 [L<sup>2</sup>T<sup>-1</sup>] is the water diffusivity,  $\epsilon = \theta^{1/3}$  [-] represents tortuosity (Millington and Quirk,  
 106 1961), and  $\delta_{ij}$  [-] is the Kronecker delta function.

107 In order to mimic a periodical repetition of the meanders in  $x$  direction and  
 108 eliminate potential boundary effects, a periodic boundary condition (Eq. (S3d)) is used  
 109 at  $\Omega_u$  and  $\Omega_d$ . This type of boundary condition can produce the periodic nature of the  
 110 model domain, flow field as well as the HZ that repeats for each meander bend (Gomez-  
 111 Velez et al., 2017). However, in order to explore the local HZ that is caused by the HEFs  
 112 at the studied meander:  $0 < x < \lambda$  (i.e., bold black line along the meander in Fig. S2a),  
 113 the conservative in-stream concentration is given by

114 
$$C_s(t) = \begin{cases} 1 & \text{if } x \in [0, \lambda] \cap \Omega_m \\ 0 & \text{else} \end{cases} \quad (\text{S5})$$

115 According to Eq. (S5), the river concentrations are assigned as an open boundary  
 116 condition along the studied meander with the external concentration mimicking the  
 117 concentration of the tracer (100% of stream water). Then the concentration of the pore  
 118 water within the aquifer represents the fraction of water inflow from river at any given  
 119 location and time.

### 120 **S3 Model of residence time distribution**

121 The residence time distribution (RTD) in the HZ describes the characteristic time  
 122 scale over which water or solutes are exposed to the biogeochemical conditions within  
 123 the hyporheic sediment. RTD is controlled by the advective and dispersive  
 124 characteristics of the system. Similar to Gomez-Velez et al. (2017), here we focus on  
 125 the orders of moment of RTD that represent the mean residence time distribution:

126 
$$\mu_n(\mathbf{x}, t) = \int_0^\infty \tau^n \rho(\mathbf{x}, t, \tau) d\tau \quad n = 0, 1, \dots \quad (\text{S6})$$

127 Where  $\mu_n(\mathbf{x}, t)$  [T<sup>n</sup>] is the  $n$ -th moment,  $\rho(\mathbf{x}, t, \tau)$  [T<sup>-1</sup>] is the residence time distribution,

128  $\tau$  [T] is residence time, and  $\mu_0 = 1$ . The first moment of RTD ( $\mu_1(\mathbf{x}, t)$ ) is the mean  
 129 residence time distribution at a given location and time, which can be used to evaluate  
 130 the transient variation of RTD. Here, we used the approach provided by Gomez-Velez  
 131 et al. (2017) where the moments of RTD are calculated by a form of the advection-  
 132 dispersion equation following

$$133 \quad \frac{\partial(H\theta\mu_n)}{\partial t} = \nabla \cdot (\mathbf{D}\nabla\mu_n - \mathbf{Q}\mu_n) + nH\theta\mu_{n-1} \quad (\text{S6a})$$

$$134 \quad \mu_n(\mathbf{x}, t=0) = \mu_{n,0}(\mathbf{x}) \quad (\text{S6b})$$

$$135 \quad \mathbf{n} \cdot (\mathbf{Q}\mu_n - \mathbf{D}\nabla\mu_n) = 0 \text{ for } \Omega_v \quad (\text{S6c})$$

$$136 \quad \mu_n(x_u, y, t) = \mu_n(x_d, y, t) \text{ for } \Omega_u \text{ and } \Omega_d \quad (\text{S6d})$$

$$137 \quad \mu_n(\mathbf{x}, t) = 0 \text{ for } \Omega_{in} \quad (\text{S6e})$$

$$138 \quad \mathbf{n} \cdot (\mathbf{Q}\mu_n - \mathbf{D}\nabla\mu_n) = 0 \text{ for } \Omega_{out} \quad (\text{S6f})$$

139 where  $\mu_{n,0}(\mathbf{x}, t)$  is the initial condition of the  $n$ -th RTD that is calculated by the base  
 140 flow condition (steady forcing before the arrival of flood event), while the upstream  
 141 and downstream boundaries are assigned periodic boundary conditions (Eq. (S6d). As  
 142 we ignore the vadose zone, the RT is defined as the time since the water entered the  
 143 model domain from the river. Thus,  $n$ -th RTD at the inflow river boundary is zero (Eq.  
 144 (S6e). A flow boundary is used for the region where the water exits the model domain  
 145 (Eq. (S6f)).

#### 146 **S4 Metrics**

147 We used the following dimensionless metrics to quantify the effects of bank  
 148 slope on the response of the dynamic hyporheic zone: (i) hyporheic exchange flux along  
 149 the river, (ii) in-valley penetration distance (i.e., the distance the river water penetrates  
 150 into the aquifer), (iii) the area of the HZ (i.e., the area of the aquifer exposed to river  
 151 water), and (iv) RTD and flux-weighted relative RT of HZ water discharging into the  
 152 river. In this section, we briefly define and describe each of these terms.

153 S4.1 Hyporheic exchange flux

154 Exchange flux from the river to the HZ ( $Q_{in, HZ}$ ) and from the aquifer to the river  
 155 ( $Q_{out, HZ}$ ) was defined as:

156 
$$Q_{in, HZ}(t) = - \int_{\partial\Omega_{in, HZ}(t)} \mathbf{Q}(\mathbf{x}, t) \cdot \mathbf{n} ds \quad (S7a)$$

157 
$$Q_{out, HZ}(t) = - \int_{\partial\Omega_{out, HZ}(t)} \mathbf{Q}(\mathbf{x}, t) \cdot \mathbf{n} ds \quad (S7b)$$

158 where  $\Omega_{in, HZ}(t)$  and  $\Omega_{out, HZ}(t)$  correspond to the inflow and outflow boundaries along  
 159 the meander of interest (black line along the river boundary in Fig. S2a). The net flux  
 160 from the aquifer into the river ( $Q_{net, HZ} = Q_{out, HZ} - Q_{in, HZ}$ ) can be expressed in  
 161 dimensionless terms following Gomez-Velez et al. (2017) using  $Q_{in, HZ}^*(t) = Q_{in, HZ}$   
 162  $(t)/(K\bar{H}_s^2)$ ,  $Q_{out, HZ}^*(t) = Q_{out, HZ}(t)/(K\bar{H}_s^2)$ , and  $Q_{net, HZ}^*(t) = Q_{net, HZ}(t)/(K\bar{H}_s^2)$ . Note that  
 163 these dimensionless fluxes are proportional to the integrated head gradient between the  
 164 river stage and the adjacent aquifer along the river boundary.

165 S4.2 Hyporheic zone area

166 Dynamic changes of the river-aquifer interface and pressure distribution along  
 167 the SWI induce variations of the flow field and changes to the HZ as represented by  
 168 area (i.e., the aquifer area exposed to river water) and penetration distance (i.e., how far  
 169 river water infiltrates into the aquifer) during the flood event. These are useful metrics  
 170 for assessing the opportunity for biogeochemical and geochemical reactions induced by  
 171 hyporheic exchange. Here we use a geochemical definition of HZ proposed by Triska  
 172 et al. (1989), that defines the HZ as the area within the alluvial valley that contains more  
 173 than 50% stream water ( $C(\mathbf{x}, t) > 0.5$ ). It can be calculated using

174 
$$A(t) = \iint a(\mathbf{x}, t) dx dy \quad (S8a)$$

175 
$$a(\mathbf{x}, t) = \begin{cases} 1 & \text{if } C(\mathbf{x}, t) \geq 0.5 \\ 0 & \text{if } C(\mathbf{x}, t) < 0.5 \end{cases} \quad (S8b)$$

176 where  $A(t)$  [ $L^2$ ] is the area of the HZ. The dimensionless area is then defined similar to



177 Gomez-Velez et al. (2017) as  $A^*(t) = A(t)/\lambda^2$  and the dimensionless variation of HZ area  
178 relative to base flow conditions can be calculated by  $A^{**}(t) = A^*(t) - A^*(0)$ , where  $A^*(0)$   
179 is the initial area of HZ in baseflow condition.

#### 180 S4.3 Penetration distance of the hyporheic zone

181 The maximum penetration distance  $d(t)$  of river water into the HZ in the direction  
182 perpendicular to the axis of the river can be calculated by the maximum  $y$  coordinate of  
183 the HZ. Similar to Gomez-Velez et al. (2017), we focus on the evolution of the  
184 dimensionless term of  $d^{**}(t) = d^*(t) - d^*(0)$ , where  $d^*(t) = d(t)/\lambda$ .

#### 185 S4.4 Residence time

186 The difference in mean residence time distribution between a sloping and a vertical  
187 riverbank model was calculated by  $\mu_r^*(\mathbf{x}, t) = \log_{10}(\mu_{\tau-s}(\mathbf{x}, t)/\mu_{\tau-l}(\mathbf{x}, 0))$ .  $\mu_r^* < 0$  indicating  
188 that RT was overestimated in these areas when ignoring the bank slope while  $\mu_r^* > 0$   
189 indicating the contrary. Furthermore, a representative value of the flux-weighted ratio  
190 of mean RT to mean RT under baseflow conditions along the river boundary is given  
191 by:  $\mu_{out}^*(x, t) = \mathbf{n} \cdot \mathbf{Q}_{out}^*(x, t) \log_{10}(\mu_{\tau}(x, t)/\mu_{\tau}(x, 0))$ , which indicates aquifer discharge of  
192 younger water with relatively short travel times (values smaller than zero) or older  
193 water with longer travel times within the alluvial aquifer as compared to the baseflow  
194 conditions.

195

#### 196 **References**

197 Bear, J., and Cheng, A. H. D.: Modeling groundwater flow and contaminant transport,  
198 Vol. 23, P. 83, Dordrecht: Springer, 2010.

199 Cooper, H. H., and Rorabaugh, M. I.: Ground-water movements and bank storage due  
200 to flood stages in surface streams, Report of Geological Survey Water-Supply, P.  
201 1536-J, US Government Printing Office, Washington, United States, 1963.

202 Gomez-Velez, J. D., Wilson, J. L., Cardenas, M. B., and Harvey, J. W.: Flow and  
203 residence times of dynamic river bank storage and sinuosity-driven hyporheic  
204 exchange, *Water Resources Research*, 53, 8572-8595, 2017.

205 Millington, R. J., and Quirk, J. P.: Permeability of porous solids, *Transactions of the*  
206 *Faraday Society*, 57, 1200-1207, 1961.

207 Schmadel, N. M., A. S. Ward, C. S. Lowry, and J, M. Malzone.: Hyporheic exchange  
208 controlled by dynamic hydrologic boundary conditions, *Geophysical Research*  
209 *Letters*, 43, 4408-4417, 2016.

210 Triska, F. J., Kennedy, V. C., Avanzino, R. J., Zellweger, G. W., & Bencala, K. E.:  
211 Retention and transport of nutrients in a third-order stream in northwest California:  
212 Hyporheic processes, *Ecology*, 70 (6), 1893-1905, 1989.

213